Effect of GIA models with 3D composite mantle viscosity on GRACE mass balance estimates for Antarctica

Wouter van der Wal[a,*], Pippa Whitehouse[b], Ernst Schrama[a]

[a]Aerospace Engineering, Delft University of Technology, Kluyverweg 1, 2629 HS, Delft, Netherlands

[b]Department of Geography, Durham University, Lower Mountjoy, South Road, Durham, DH1 3LE, United Kingdom

*Corresponding author, E-mail address: w.vanderwal@tudelft.nl, phone number: +31 152782086

Abstract

Seismic data indicate that there are large viscosity variations in the mantle beneath Antarctica. Consideration of such variations would affect predictions of models of Glacial Isostatic Adjustment (GIA), which are used to correct satellite measurements of ice mass change. However, most GIA models used for that purpose have assumed the mantle to be uniformly stratified in terms of viscosity. The goal of this study is to estimate the effect of lateral variations in viscosity on Antarctic mass balance estimates derived from the Gravity Recovery and Climate Experiment (GRACE) data. To this end, recently-developed global GIA models based on lateral variations in mantle temperature are tuned to fit constraints in the northern hemisphere and then compared to GPS-derived uplift rates in Antarctica.

We find that these models can provide a better fit to GPS uplift rates in Antarctica than existing GIA models with a radially-varying (1D) rheology. When 3D viscosity models in combination with specific ice loading histories are used to correct GRACE measurements, mass loss in Antarctica is smaller than previously found for the same ice loading histories and their preferred 1D viscosity profiles. The variation in mass balance estimates arising from using different plausible realizations of 3D viscosity amounts to 20 Gt/year for the ICE-5G ice model and 16 Gt/year for the W12a ice model; these values are larger than the GRACE measurement error, but smaller than the variation arising from unknown ice history. While there exist 1D Earth models that can reproduce the total mass balance estimates derived using 3D Earth models, the spatial pattern of gravity rates can be significantly affected by 3D viscosity in a way that cannot be reproduced by GIA models with 1D viscosity. As an example, models with 1D viscosity always predict maximum gravity rates in the Ross Sea for the ICE-5G ice model, however, for one of the three preferred 3D models the maximum (for the same ice model) is found near the Weddell Sea. This demonstrates that 3D variations in viscosity affect the sensitivity of present-day uplift and gravity rates to changes in the timing of the ice history. In particular, low viscosities ($<10^{19}$ Pas) found in West Antarctica make the mantle very sensitive to recent changes in ice thickness.

Keywords

Glacial rebound, mantle rheology, viscosity, time-variable gravity, GRACE, Antarctica

1. Introduction

Measurements of time-variable gravity from the GRACE satellite mission show continuous decrease of mass over Antarctica since the GRACE launch in 2002 (Velicogna and Wahr 2006, King et al. 2012). A large part of the gravity change reflects mass redistribution in the solid Earth as the viscous mantle responds to past changes in ice load, a process known as Glacial Isostatic Adjustment (GIA). In order to determine present ice mass change in Antarctica GRACE measurements have to be corrected for GIA, either: (i) by employing a geophysical model for GIA (e.g. Velicogna and Wahr 2006, Chen et al. 2009, King et al.

2012), or (ii) by employing other datasets with different sensitivities to GIA and ice melt such as GPS or satellite altimetry (Wahr et al. 1995; Wahr et al. 2000; Riva et al. 2009; Wu et al. 2010; Wang et al. 2013; Sasgen et al. 2013; Gunter et al. 2014). Method (ii) has the advantage that it is not necessary to rely on geophysical models of GIA. However, it requires accurate knowledge of firn compaction to be able to relate volume changes measured by satellite altimetry to mass changes measured by GRACE. Also, satellite altimetry, specifically ICESat, suffers from inhomogeneous temporal and spatial coverage, cloud cover, detector saturation and inter-campaign biases (Shuman et al. 2006; Shepherd et al. 2012). Inversion of space-geodetic data (Wu et al. 2010; Sasgen et al. 2013) is sensitive to data distribution, and spurious signals can be generated in areas with fewer data. Finally, method (ii) does not make use of many key constraints on the GIA process, such as historic sea-level indicators, geomorphological, geological and glaciological constraints on the shape and thickness of the ice sheet, and knowledge of the interior of the Earth below Antarctica.

Considering the advantages and disadvantages of each method, there is merit in pursuing both methods in parallel for estimating present-day ice mass balance. In this study we select method (i) and focus on the unknown structure of the Earth and how this affects predicted gravity changes due to GIA.

Most GRACE mass balance estimates for Antarctica that rely on method (i) have assumed that deformation in the Earth's mantle can be parameterized using a viscosity distribution that only varies with depth (e.g. Velicogna and Wahr 2006, Chen et al. 2009, King et al. 2012). In the following, this parameterization will be referred to as 1D viscosity. However, from surface wave data it is clear that the mantle is very different beneath East and West Antarctica (Ritzwoller et al. 2001; Danesi and Morelli 2001). Assuming that differences in seismic velocities stem from differences in mantle temperature, Kaufmann et al (2005) suggest that a large difference in mantle viscosity exists between East and West Antarctica. Such differences could have a large effect on (regional) mass balance estimates for Antarctica and the interpretation of GPS and altimetry data because present-day uplift rates are sensitive to the local viscous relaxation time. Below we discuss previous studies and open questions.

Kaufman et al. (2005) showed that the inclusion of 3D viscosity within a GIA model results in an uplift rate pattern that is similar to a 1D viscosity model. A et al. (2013) have computed gravity rates for a compressible GIA model with 3D viscosity and found that the effect on mass change estimates is only mildly different compared with a 1D model. Differences between 1D and 3D models therefore seem to be smaller than the uncertainty resulting from poor knowledge of the ice loading history. However, Kaufman et al. (2005) and A et al. (2013) only considered one 3D viscosity distribution for Antarctica, while there are actually many unknowns associated with deriving 3D viscosity variations from seismic information (e.g. Ivins and Sammis 1995; Trampert and van der Hilst 2005). In order to fully investigate the effect of 3D viscosity in GIA models, the uncertainty in producing 3D viscosity maps should be considered, including the effects of different flow laws. In our approach we take into account the two main types of deformation in the mantle (diffusion and dislocation creep) in a so-called composite rheology (Gasperini et al. 1992; van der Wal et al. 2010). Due to the difficulty of modelling the gradient in Earth structure that exists between East and West Antarctica, regional GIA models, which adopt a 1D viscosity profile, have been used to investigate the GIA signal in specific regions of Antarctica (e.g. Ivins et al. 2011; Nield et al. 2012, 2014). Such models are likely to continue to be used because they can achieve the necessary spatial resolution for studying the Earth's response to changes in ice loading on a regional scale. Therefore, one of our aims is also to produce a range of viscosity maps that can be used in regional GIA studies that adopt a 1D viscosity profile.

Clearly GIA models with 3D viscosity are more computationally expensive than GIA models with 1D viscosity, and therefore it is important to determine whether it is necessary to use 3D models to correct GRACE mass balance estimates, or whether 1D models are sufficient (see section 3.5). Maybe the range of mass balance estimates produced using a suitably wide range of 1D GIA models contains the mass balance estimate that would be produced using a 3D Earth model, or maybe there are important regional differences between the mass change predicted by a 1D model and a 3D model?

In summary the research questions to be answered in this study are:

1. What is the effect of using GIA models with different 3D viscosity distributions on Antarctic mass balance estimates derived from GRACE?
2. What range of lateral (effective) variations in viscosity can be expected beneath Antarctica?
3. Can the gravity rate pattern from GIA models with 3D rheology be reproduced by a GIA model with 1D rheology?

In this study the free-air gravity anomaly rate is computed at the Earth's surface, and this will be referred to in the following as simply the gravity rate. Section 2 describes the most important features of the numerical GIA model and ice loading histories used. This section is followed by the presentation of viscosity maps for the preferred 3D models and a comparison of model predictions with GPS data in Antarctica. Finally, mass balance estimates and a comparison of predictions from 1D and 3D GIA models are presented.

2. Methods

2. 1 Finite-element model

The GIA model is based on the commercial finite-element software ABAQUS^{TM}, following Wu (2004). Elements have a 2˚ x 2˚ resolution at the surface and, as described in that paper, self-consistent sea levels and self-gravitation are included, but not compressibility, geocenter motion and shoreline migration. Viscous parameters, as described below, are defined for layers with boundaries at 35, 70, 120, 230, 400, 670, 1170 and 3480 km depth. Elastic parameters are as in van der Wal et al. (2013) with boundaries taken at the major seismic discontinuities at 400, 670, 1170 and 3480 km depth as well as at 120 km depth. Density and rigidity for each layer are obtained by volume-averaging PREM layers with small adjustments in order to better match density jumps. The model is extended to include the two main types of deformation in the mantle: diffusion creep and dislocation creep (van der Wal et al. 2010). Here we use a composite rheology (Gasperini et al. 1992; van der Wal et al. 2010) based on the flow laws for diffusion and dislocation creep in olivine. We assume that olivine is the main mantle material and consider variations in grain size and water content. By varying these parameters we introduce large variations in the viscosities that are derived from thermal anomalies. In addition, because strain rate for dislocation creep depends on stress, effective viscosity varies with stress and hence with time. Including dislocation creep results in small present-day uplift-rates, but this is partly countered by using a combination of diffusion and dislocation creep (van der Wal et al. 2010).

Individual strain components are calculated as (van der Wal et al. 2013):

$$\varepsilon = B_{diff} q \Delta t + B_{disl} q^n \Delta t , \tag{1}$$

where B_{diff} and B_{disl} are creep parameters computed from the flow law for diffusion and dislocation creep, respectively, t is time, n is the stress exponent, and q is the von Mises stress $q = \sqrt{\frac{3}{2}\sigma'_{ij}\sigma'_{ij}}$ with σ'_{ij} an element of the deviatoric stress tensor. Above 400 km, where olivine is the main mantle material, the olivine flow laws from Hirth and Kohlstedt (2003) are used to compute B_{diff} and B_{disl}:

$$B = A d^{-p} fH_2O^r e^{\alpha\varphi} e^{-\frac{E+PV}{RT}} , \tag{2}$$

in which A and α are constants, d is the grain size, fH_2O is water content, φ is melt fraction, E is activation energy, P is pressure, V is activation volume, R is the gas constant, T is absolute temperature, and p and r are the grain size and water fugacity exponents, respectively. Of these, E, V, p, r and A are taken from Hirth and Kohlstedt (2003) for either diffusion or dislocation creep. The pressure as a function of depth is calculated by assuming that the pressure gradient is equal to 0.033 GPa/km (Keary et al. 2009). Grain size, water content and temperature are unknown and will be varied as described later, while melt content is set to zero. It has been shown that in a high-temperature region such as Iceland, melt content as modelled by equation (2) has a relatively small influence on effective viscosity compared to grain size and water content (Barnhoorn et al. 2011a). Effective viscosity can be calculated by (van der Wal et al. 2013):

$$\eta_{eff} = \frac{1}{3B_{diff} + 3B_{disl}q^{n-1}} \tag{3}$$

The top 35 km of the Earth are assumed to be non-viscous. Below that, the effective viscosity determines whether an element is responding viscously or not, and hence whether it can be considered part of the lithosphere. For the Earth layers below 400 km, values for B_{diff} and B_{disl} are assumed to vary only radially because the olivine flow laws of Hirth and Kohlstedt (2003) do not hold in this region. B_{diff} and B_{disl} values for these depths are taken from a 3D GIA model that has been tuned to fit a range of relative sea-level data (van der Wal et al. 2010),

Temperature is derived in two different ways, from surface heat flow data (labelled HF) and from a global seismic model (labelled SEIS). The most important steps in obtaining the temperature maps are described in the following, but more information is given in van der Wal et al. (2013). In the HF approach surface heat flow maps are used from Shapiro and Ritzwoller (2004). They extrapolated heat flow data from Pollack et al. (1993) to areas where none was available. The extrapolation is based on a shear wave velocity model and assumes a thermally homogeneous crust. Geotherms are computed by integrating the equation for 1D steady-state heat transfer, assuming constant heat generation.

Because very few heat flow measurements exist for Antarctica, standard deviations in inferred heatflow there, as derived by Shapiro and Ritwzoller (2004), are large. Instead of using this standard deviation to determine uncertainties associated with the temperature distribution, we use a second, independent, approach to obtain an estimate of temperature. In the SEIS approach laterally varying velocity anomalies from Grand (2002) are converted to temperature using the depth-dependent temperature derivative of seismic wave velocities given in Karato (2008). Here, it is assumed that all seismic anomalies are due to thermal anomalies, while in reality chemical heterogeneity has an influence. In the upper mantle the effect of chemical heterogeneity is probably smaller than the effect of thermal anomalies (Cammarano et al. 2011), but nevertheless it can influence GIA predictions (Wu et al. 2013). Thus SEIS temperature estimates are an upper bound for lateral variations in temperatures. Large differences exist between different tomography models (Schaeffer and Lebedev, in press), and hence will lead to differences in thermal maps. Our use of two different methods to obtain thermal anomalies captures some of the variation arising from uncertainty in the approaches, but the uncertainty arising from different seismic tomography models is an important target for future work. Another interesting approach is that of Priestley and McKenzie (2013), who estimate viscosity directly from shear wave velocity models and geophysical and petrological data.

We found an error in the calculation of the SEIS temperature model in van der Wal et al. (2013), which resulted in the temperatures being too high at shallow depths and too low for deeper layers. The effect on sea-level curves is small for the best fitting models, but uplift rates were affected more therefore the recalculated rates are shown in section 3.1. The two methods for computing temperatures result in markedly different temperature distributions with SEIS having lower temperatures than HF.

The final two parameters that must be defined within the Earth model are grain size and water content. Grain size is varied between 1, 4 and 10 mm, which is the range found for kimberlites and peridotites (Dijkstra et al. 2002). Water content is varied between a fully wet (1000 ppm H_2O) and a fully dry state. Varying the mantle temperature (SEIS and HF), grain size (1/4/10 mm) and water content (wet/dry) results in a total of 2x3x2=12 combinations of mantle parameters that are investigated for each ice loading history (see next section).

Effective viscosities are calculated for each ice-Earth model combination, and will vary over both space and time. Variations in space are caused by spatial variations in temperature and stress. Variations in time are due to the non-linear part of the dislocation creep flow law (second term of equation (1)), which has been shown to affect viscosity by two orders of magnitude during the glacial cycle, neglecting the influence of background stress (Barnhoorn et al. 2011b).

2.2 Ice models

We use two different ice loading histories for Antarctica: ICE-5Gv1.2 (Peltier 2004; referred to as ICE-5G) and W12a (Whitehouse et al. 2012a,b), both of which have previously been used to correct GRACE measurements for Antarctic GIA effects. The Antarctic component of the more recent ICE-6G model was published during preparation of this manuscript (Argus et al. 2014) but the ice-loading history associated with this model was not available for comparison with earlier models at the time the manuscript was prepared. We assume that ICE-5G and W12a span reasonable possible ice loading variations (see also Ivins et al. 2013, figure 2) and do not use the Ivins et al (2013) ice-loading history in order to limit our computational effort. An important limitation of all three ice-loading histories is that they are tuned to fit to sea-level or uplift data assuming a laterally homogeneous Earth. In future work 3D viscosity should be considered when developing ice-loading histories.

The ICE-5G and W12a models have been interpolated onto the 2° x 2° equiangular grid of the finite-element model, and ice thickness changes are defined at 1000 year intervals between 20 ka BP and the present. Prior to 20 ka BP ice thickness is assumed to increase linearly over 90 ka. The main differences between W12a and ICE-5G are:

- W12a incorporates a larger number of palaeo ice thickness constraints, derived from exposure age dating, which were not available when ICE-5G was developed
- W12a was developed using a numerical ice-sheet model while ICE-5G was directly tuned to fit field observations
- W12a makes use of near-field relative sea-level data to fine-tune the model whereas ICE-5G is tuned using a global relative sea-level dataset

As a result of these differences, the total meltwater contribution from Antarctica since the Last Glacial Maximum (LGM) is smaller in the W12a model than the ICE-5G model. Both models in fact define global ice thickness changes throughout the last glacial cycle, but outside Antarctica W12a is identical to the ICE-5G loading history.

These two ice models are used to solve the sea-level equation (Farrell and Clark 1976) and hence determine gravitationally self-consistent global variations in relative sea level and Earth deformation throughout the last glacial cycle at 1000 year time steps. For ICE-5G, present-day uplift rates are obtained by numerical differencing of the predicted solid earth displacement 1000 years before and after the present. Hence the rates are centred on present. For the W12a model the derivative is calculated over a different interval because there are ice thickness changes up to 500 years before present which would result in large elastic effects contributing to the uplift rate if it was calculated in the same way as for ICE-5G. The uplift rate for the W12a model is therefore calculated as the difference in displacement between present and 100 years in the future. This only requires the addition of one extra time step in the computation and is found to be sufficiently accurate. The difference between rates centered at 500 and at 50 years in the future in terms of uplift rate is at most 1.1 mm/year in areas of maximum uplift rate and less than a few tenths of mm/year outside those areas. It follows that rates centered at 50 years in the future will differ from rates centered at present by much less than this amount.

3. Results and Discussion

The preferred 3D GIA models, based on comparison with constraints on northern hemisphere GIA, are presented in Section 3.1. Section 3.2 presents maps of effective viscosity for the preferred 3D GIA models. Section 3.3 compares uplift rates from the 3D models with GPS-measured uplift rates in Antarctica. The effect on GRACE mass balance estimates is discussed in section 3.4. Finally, comparisons between gravity rates from 1D and 3D GIA models are made in section 3.5.

3.1 Preferred 3D GIA models

The 12 3D models predict very different uplift rates and gravity rates. In order to select which of the models can result in realistic uplift rates, we compare model output to observations in regions where GIA uplift rates area clearly observed, i.e. Scandinavia and North America (figure 1). In the absence of other information on flow law parameters suitable for Antarctica, we assume that the flow law parameters that result in realistic uplift rates in the northern hemisphere also result in reasonable uplift rates in Antarctica. For this comparison the ICE-5G model is used; the W12a ice model would give nearly identical results because its loading history is identical to ICE-5G in the northern hemisphere and the effect of using a different Antarctic melt history on uplift rates in the northern hemisphere is negligible. All the models predict uplift rates that are too low in Scandinavia and North America when ICE-5G is used, a known result for models with non-linear rheology and, to a lesser extent, composite rheology (van der Wal et al. 2010).

This misfit decreases in Scandinavia when the load history is derived from a paleo ice height model that is not based on an earth model with Maxwell rheology and 1D viscosity (van der Wal et al. 2013), however, the maximum observed uplift rates are still not reproduced in this case (figure 1b). It appears from the figure that under certain conditions an increase in grain size could increase the predicted uplift rate but this was not found to be the case in previous work (van der Wal et al., 2013). Therefore, for this study we simply select the models that yield the highest uplift rates even though they are still somewhat below the measured maximum uplift rate. For North America and Scandinavia the best model is a dry rheology with 10 mm grain size combined with temperature model HF (labelled HF10D). If the SEIS temperature model is accepted, a model with dry rheology and 4 mm grain size (labelled S4D) gives the largest uplift rates.

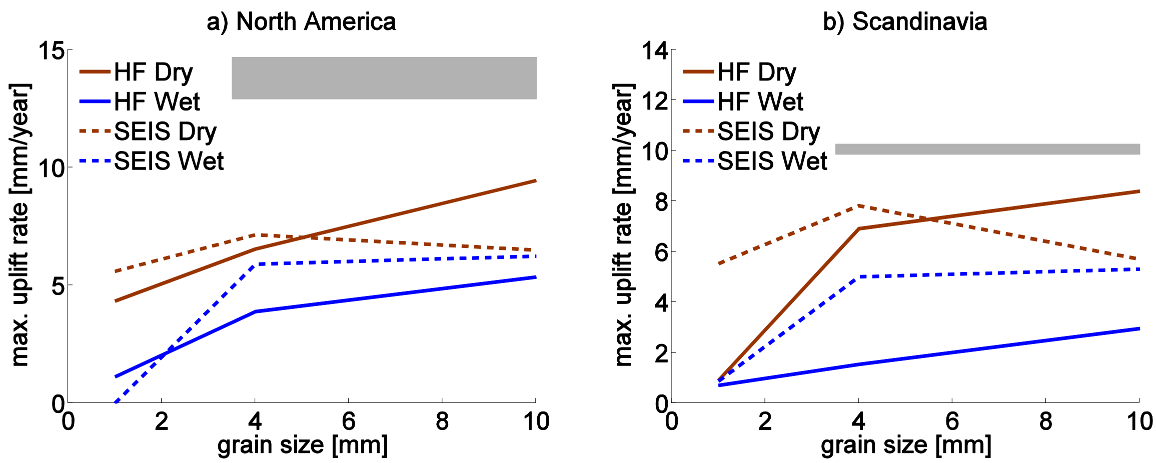

Figure 1: Maximum uplift rate for different models in North America (a) and Scandinavia (b). The grey bar indicates the maximum observed uplift rate with one standard deviation in North America and Scandinavia, according to Sella et al. (2007) and Lidberg et al. (2007), respectively. For figure 1a the ICE-

5G ice model is used and for figure 1b an ice model is used that was developed independently from GIA observations and mantle viscosity, see van der Wal et al. (2013).

The model predictions were also compared with relative sea-level data in Fennoscandia (van der Wal et al. 2013). In that case the best model is based on the HF temperature model in combination with a wet rheology and 10 mm grain size. Because the HF10W model gives a very poor fit to uplift rates in Scandinavia (figure 1b) we instead adopt the S10W model as our third preferred model. This is a reasonable trade-off since the S10W model only gives a slightly worse fit to the relative sea-level data than the HF10W model. The three models HF10D, S4D, and S10W will be used to investigate the range in predictions one can get from 3D models.

3.2 Effective viscosity maps

Maps of effective viscosity in Antarctica are plotted for the first preferred model (HF10D) in figure 2 using W12a at time 14 ka before present. Recall that according to equation (3) effective viscosity is a function of the (von Mises) stress which also depends on the ice model. A viscosity map for ice model ICE-5G, as well as for a different epoch (present) is provided in supplementary material A.1. These additional viscosity maps are similar to figure 2, but viscosity can be up to two orders of magnitude smaller due to larger ice thickness changes prescribed by the ICE-5G ice model and up to one order of magnitude larger due to the lower stresses at present compared to 14 ka before present. More discussion is provided in the supplementary material A.1 and an extensive analysis of temporal changes in viscosity is presented in Barnhoorn et al. (2011b).

In figure 2 it can be seen that, at a depth of 52 km, viscosity is low ($< 10^{20}$ Pa s) in West Antarctica and the northern Antarctic Peninsula, while East Antarctica has high viscosity ($> 10^{24}$ Pa s). At 95 km depth for model HF10D, viscosity in most of East Antarctica is too high for any viscous deformation, with the exception of the coastal parts of Dronning Maud Land. At depths of 145 km, viscosities in West Antarctica increase to around 10^{21} Pa s while viscosities around much of coastal East Antarctica approach the same value. Finally, at 200 km depth viscosities are low enough for viscous deformation to occur beneath the whole of East Antarctica. Lateral variations at this depth are small because the temperature is determined more by the mantle adiabat than the value of surface heat flow.

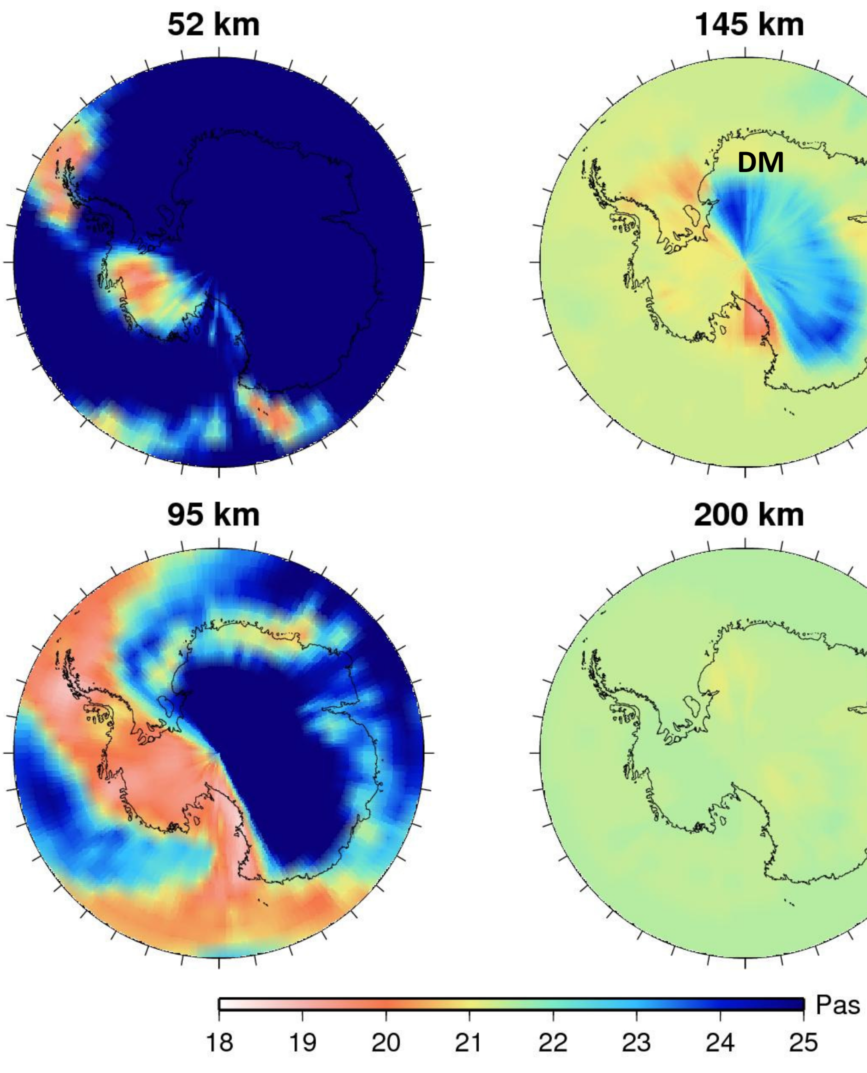

Figure 2: Effective viscosity at 4 depths for preferred model HF10D, as derived using the W12a ice loading history. DM denotes Dronning Maud Land.

Figure 3 shows the viscosity for model S10W, which provides the second best-fit to historic sea levels in Scandinavia and second best fit to uplift rates in Antarctica (next section). For this model temperatures are derived from seismic velocity anomalies and the flow laws are those for wet olivine (see details in van der Wal et al. (2013)). Because of low temperatures at shallow depths (see section 2.1), effective viscosities down to 95 km are large enough that no viscous deformation will occur across the whole of Antarctica, except in the western Ross Sea, in this model. At 145 km depth the viscosity beneath the Antarctica Peninsula and beneath the Ross Ice Shelf is lower than 10^{18} Pa s, which corresponds to relaxation times on the order of decades. This is somewhat below estimates in a recent study in the northern Antarctic Peninsula which found that viscosities of 10^{18} Pa s are required in order to match observed uplift rates following the 2002 breakup of the Larsen B Ice Shelf (Nield et al. 2014). However, we note that transient creep may be in operation over these time scales, as suggested by experimental data (Faul and Jackson 2005). Such a process is not considered here or by Nield et al. (2014), although the stress-dependence in equation (1) makes the viscosity weakly time-dependent in this study. At 200 km depth, viscosity in some coastal regions of East Antarctica, e.g. Dronning Maud Land, drops to 10^{21} Pa s or below for the first time.

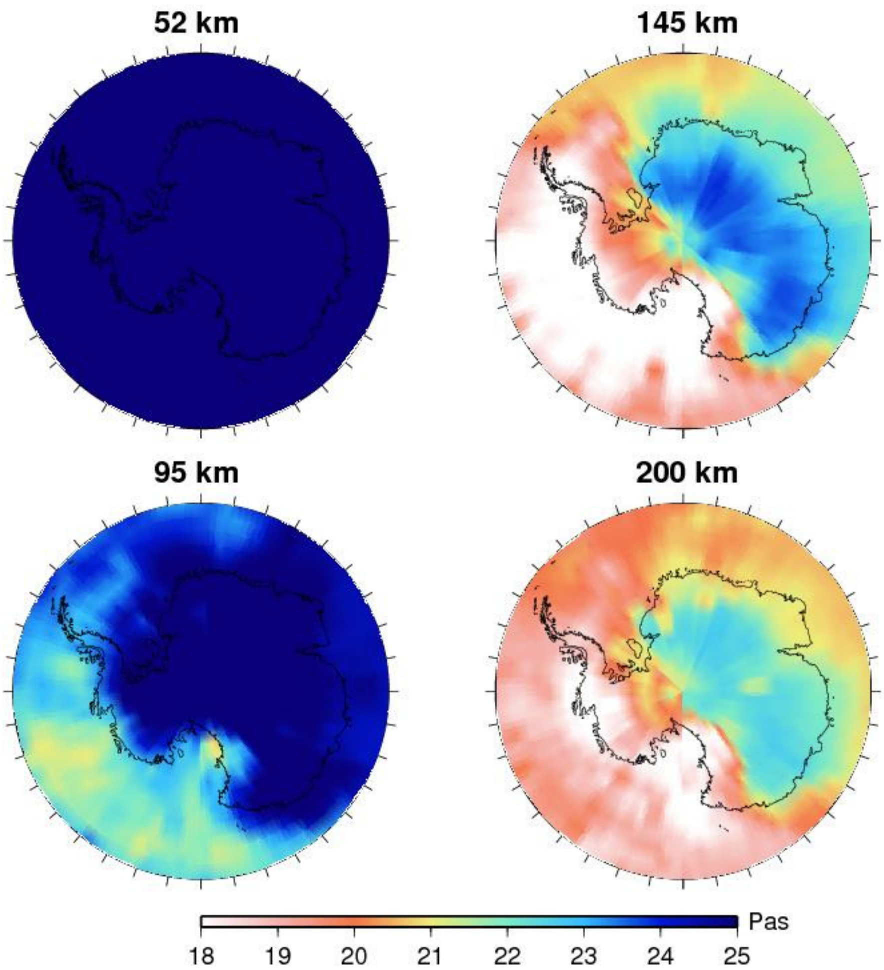

Figure 3: Effective viscosity at 4 depths for preferred model S10W, as derived using the W12a ice loading history.

The relationships between viscosity variations and depth below Antarctica are shown in Figure 4. Below 200 km the model based on heat flow shows a viscosity slightly increasing with depth, its value close to that of a two-layer approximation of VM2, where VM2 is the viscosity profile that is used to construct the ICE-5G ice loading history (Peltier 2004). By comparing the SEIS models it can be seen that the effect of larger grain size, which acts to increase viscosity, can be more than compensated by having a wet instead of a dry rheology.

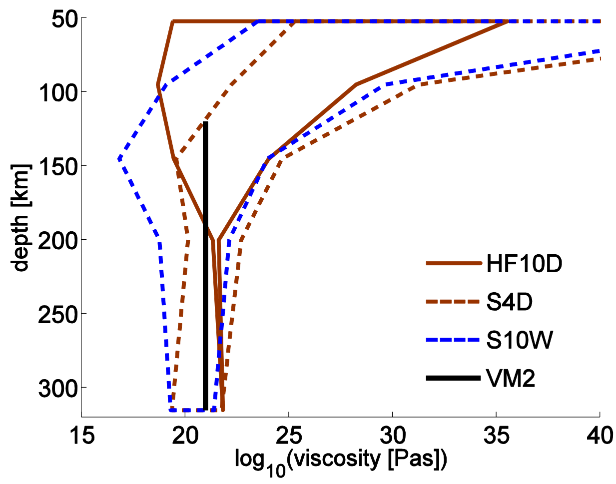

Figure 4: Viscosity ranges below Antarctica as a function of depth, averaged over all time steps, for models based on the W12a ice loading history.

Both the wet rheology of model S10W and the small grain size in model S4D result in very low viscosities in the flow laws of Hirth and Kohlstedt (2003), and consequently too small uplift rates in Fennoscandia and North America (Figure 1). However, when combined with the ICE-5G ice-loading history, these models can reproduce GPS-measured uplift rates in Antarctica better than models with a 1D rheology, as will be shown in the next section. Whether this improved fit is because the 3D models better represent the Earth structure beneath Antarctica, or whether errors in the ice and Earth models cancel out, can only be determined by independently testing the accuracy of the ice models such as in Whitehouse et al. (2012a) and Argus et al. (2014). While 3D rheology can only be constrained via GIA-related observations if the ice model is constrained independently using ice extent data, further evidence of low viscosities comes from xenoliths with olivine samples with small grain size (0.1-4 mm) and hydrous minerals; see the compilation in supplementary material A.2.

3.3 Comparison with GPS uplift rates

The 3D model predictions are compared with GPS uplift rates from Argus et al. (2014). The elastic uplift correction in that study relies on a GIA model and only corrects for long-wavelength effects. Therefore here the modeled elastic uplift correction from Thomas et al. (2011) is used for all stations. Rates on the northern Antarctic Peninsula are presumed to reflect mostly elastic uplift (Thomas et al. 2011) so they are not considered in this study, neither are stations for which the time series is shorter than 5 years. A total of 23 stations pass these criteria. The GPS uplift rates are given in ITRF2008, while the origin of the model reference frame is the instantaneous center of mass of the Earth (CM). A drift can exist between ITRF2008 and the CM frame. Such a drift manifests itself mostly as a bias between modeled and measured uplift rates. For this reason we only consider uplift rates relative to a specific site (as in van der Wal et al. 2011); in this case, the site with the smallest movement (maximum modelled uplift rate of 1.2 mm/year, across all models) which also happens to be the site with the longest time series (Mawson). The modeled uplift rate at this site is subtracted from all modeled uplift rates. This procedure also largely removes the effect of rotational feedback to GIA which is present in the measured uplift rates but absent from the modeled uplift rates.

Misfits between modelled and observed uplift rates are computed according to the following definition:

$$\chi^2 = \frac{1}{N}\sum_{i=1}^{N}\left(\frac{o_i - p_i}{\sigma_i}\right)^2, \tag{4}$$

where N is the number of observations (22), o_i are the elastic-corrected relative uplift rate observations, p_i are the predicted relative uplift rates from the models interpolated at the GPS sites and σ_i are the standard deviations from Argus et al. (2014), not including the error in the elastic correction. Misfits are listed in Table 1. In there, each ice model is combined with the three preferred 3D Earth models. For reference the table also shows results derived from the published uplift rates for each ice model, which were produced using a specific 1D earth model. For ICE-5G this is the VM2 viscosity profile; uplift rates for ICE-5Gv1.3 in combination with VM2 L90 are taken from http://www.atmosp.physics.utoronto.ca/~peltier/data.php (last accessed August 2014). For the W12a model the optimum Earth model is constrained by relative sea-level data and uplift rates are taken from Whitehouse et al. (2012b). The combination of the W12a ice model and the earth model parameters as derived in Whitehouse et al. (2012b) will be referred to as the Whitehouse et al. (2012b) model, with predictions taken from that paper. We note that both these published models were derived using a spectral GIA model, and therefore differences with the 3D model results may be due in part to the use of a finite element model in this study.

To investigate this we reproduced uplift rates from the Whitehouse et al. (2012b) model with the finite element model, using the same elastic and viscous profile as Whitehouse et al. (2012b) (supplementary material A.4). Uplift rates from the original Whitehouse et al. (2012b) model result in a misfit of 0.91, while the finite-element reproduction of this model gives a slightly larger misfit of 0.95, mainly due to the smoothing of the ice load in the lower-resolution finite-element model. This suggests that the two computational methods give comparable results. In addition, the fact that a finite-element model with 3D Earth structure (HF10D) is able to produce smaller misfits than the finite-element version of the 1D Whitehouse et al. (2012b) model indicates that the improvement is most likely due to the imposed 3D viscosity variations.

For the ICE-5G model, all 3D models result in an improved misfit. A histogram of the differences in supplementary material A.3 shows that this mainly arises due to the reduction of previously-large uplift rates at a few sites. The 3D model that gave the second-highest uplift rates in the northern hemisphere (S4D) leads to the best fit for the ICE-5G model in Antarctica. It is possible that the rheology of model S4D better reflects the rheology in Antarctica compared to models HF10D and S10W, but the small difference in misfit is unlikely to be significant in the presence of other model errors.

Table 1: Misfit between modelled uplift rates and selected GPS uplift rates from Argus et al. (2014) with elastic rate corrections from Thomas et al. (2011).

Ice model	W12a				ICE-5G			
Earth model	Whitehouse et al. (2012b)	HF10D	S4D	S10W	VM2 Peltier (2004)	HF10D	S4D	S10W
Misfit (eq. 4)	0.91	0.74	1.2	2.6	1.3	0.72	0.61	0.63

Uplift rates for the case when W12a is combined with the HF10D earth model are plotted together with the uplift rates from Whitehouse et al. (2012b) in Figure 5. The colored dots depict the elastic-corrected GPS uplift rates from Argus et al. (2014). Uplift rates for the 3D composite rheology model are smaller, as found previously for Scandinavia and North America (van der Wal et al. 2013). Smaller uplift rates can result both from lower than average viscosity leading to fast relaxation, as seen in the Amundsen Sea Sector, as well as higher than average viscosity, as found below central East Antarctica (see figure 2) where subsidence rates are reduced.

While the smaller uplift rates in the northern hemisphere underpredict observed uplift rates, the introduction of 3D structure and composite rheology improves the fit to observed rates in Antarctica. One explanation is the fact that in Antarctica composite rheology does not reduce uplift rates as much as it does in North America. The maximum uplift rate for model HF10D in Antarctica is larger than the VM2 uplift rate there, while in North America and Scandinavia the HF10D uplift rates are below the VM2 uplift rates (see van der Wal et al. 2013, figure 12). However, another explanation could be that larger variations in Earth structure exist beneath Antarctica which increases the influence of 3D rheology. Note that the uncertainty in ice models in Antarctica is larger, therefore improvements in fit are less significant.

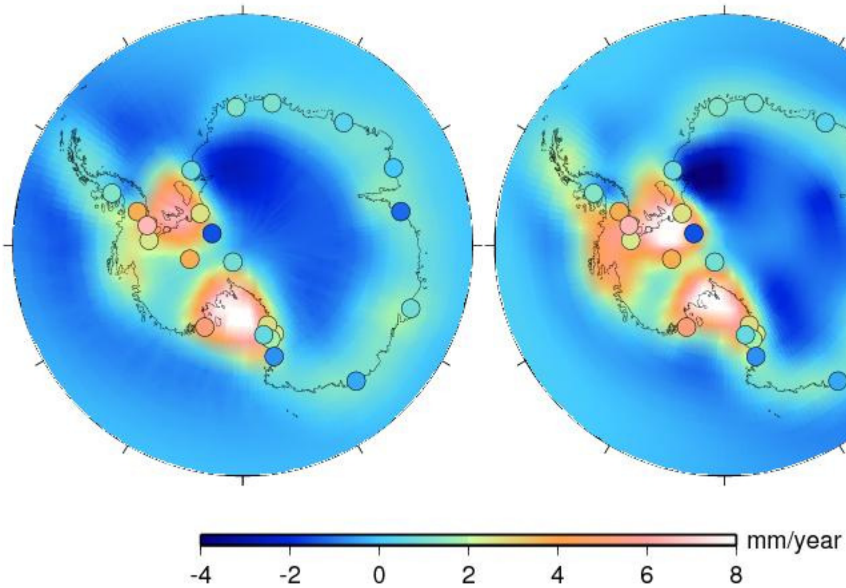

Figure 5: Uplift rate maps for the W12a ice loading history. left: 3D earth model HF10D, right: uplift rates from Whitehouse et al. (2012b).

3.4 Mass balance estimates

To obtain mass balance estimates from GRACE, we use Release 5 monthly gravity fields from the Center for Space Research spanning February 2003 to June 2013. The procedure is described in Schrama et al. (2014); a brief summary is provided in the following. The C_{20} coefficient is replaced by the values from Satellite Laser Ranging (SLR) ranging (Cheng et al. 2013) and continental water storage changes are accounted for using the GLDAS model (Rodell et al. 2004). The GRACE data are inverted for water equivalent height in 10242 globally distributed mascons. Errors are determined by propagating calibrated standard deviations of the sets of monthly coefficients into the trend estimate. Loading at degree 1 resulting in geocenter motion is not directly observed by GRACE but can be estimated indirectly by assuming that mass loss from ice sheets and glaciers adds to the oceans. The method is described in (Schrama et al. 2014) where it is found that Antarctica receives a correction of 33 Gt/year.

The mass balance estimates from GRACE are corrected for GIA to yield estimates of ice mass balance in Antarctica. Our GIA models do not include the effect of a change in the rotational potential as a result of a change in the moment of inertia due to mass redistribution. To estimate the effect we replaced the Stokes coefficients for degree 2 order 1 with values computed using a GIA model that does include rotational feedback (Peltier et al. 2012) and found a small increase in mass balance estimates of 3 Gt/year.

The mass balance derived using different GIA models is summarized in Table 2. We use the three preferred models as an indication of the possible spread in mass balance estimates resulting from unknown 3D rheology. This is not an uncertainty range in the formal sense, as we did not investigate variation in all parameters in the 3D rheology, and no statistical test with respect to the data is performed. Moreover, the ice models neglected coupling with the 3D Earth rheology, so the true spread from 3D rheology could be larger. Still we think that it is insightful to see the impact of three realizations of 3D rheology that can provide a reasonable fit to GIA observations on the northern hemisphere as well as in Antarctica.

The mass balance estimates in Table 2 are different from previous estimates partly due to an acceleration in ice melt (Velicogna 2009) and anomalous snowfall in 2009 across Dronning Maud Land (Boening et al. 2012). For the ICE-5G model, the use of the three different 3D viscosity models results in a variation in mass balance of 20 Gt/year, with most of the variation in West Antarctica, and a mean value of mass loss that is 23 Gt/year smaller than for ICE-5G/VM2. For W12a the mass balance estimates vary by 16 Gt/year, and the mean mass loss is 51 Gt/year smaller than when the (1D) Whitehouse et al. (2012b) model is used to correct GRACE. Some of this discrepancy may be accounted for by model differences: when the finite-element model is run using the 1D Earth model parameters of Whitehouse et al. (2012b) it underpredicts the signal due to GIA by 15 Gt/year (see supplementary material A.4), however, even after accounting for this, the step from 1D to 3D results is still significant. About half of the difference between the 1D and 3D models is coming from West Antarctica where the 3D models predict smaller uplift rates than the 1D Whitehouse model (see Figure 5). For East Antarctica, greater rates of ice mass gain are estimated when 3D models are used.

Table 2: Mass balance estimates for GIA models with varying Earth model parameters and different ice models. The error in the trend derived from calibrated standard deviations of the GRACE monthly gravity fields is 9.2 Gt/year for Antarctica, 3.2 Gt/year for West Antarctica, 1.9 Gt/year for the Antarctic Peninsula and 6.7 Gt/year for East Antarctica. The models in rows 5 to 7 are 1D models that best approximate the HF10D, S4D and S10W models, respectively; they are discussed further in section 3.5.

		Ice Mass Change [Gt/year]			
GIA Earth model	Ice model	All Antarctica	West Antarctica	Antarctic Peninsula	East Antarctica
HF10D	ICE-5G	-166	-147	-36	17
S4D	ICE-5G	-154	-141	-35	23
S10W	ICE-5G	-146	-135	-34	23
VM2	ICE-5G	-178	-153	-41	15
1D/HF10D	ICE-5G	-163	-145	-35	17
1D/S4D	ICE-5G	-160	-144	-34	19
1D/S10W	ICE-5G	-146	-136	-33	23
HF10D	W12a	-55	-122	-30	97

S4D	W12a	-48	-120	-25	97
S10W	W12a	-39	-117	-19	97
Whitehouse et al. (2012b)	W12a	-98	-146	-39	87

From Table 2, the maximum difference between two models that use the same earth model but different ice models is 111 Gt/year. Thus, the range in mass balance estimates resulting from variations in 3D viscosity (across our three preferred models) is less than the uncertainty caused by variations in the ice loading history (as also found by A et al. 2013), but larger than the uncertainty in the GRACE-derived trends. The range due to 3D viscosity variations is comparable to the uncertainty in 1D GIA models derived in King et al. (2012) and Ivins et al. (2013), 18 and 30 Gt/year respectively, but it is smaller than the 110 Gt/year in Barletta et al. (2008).

3.5 Approximating a 3D GIA model with a 1D GIA model

We wish to determine whether gravity rate predictions derived using a GIA model with 3D viscosity variations may be well-approximated by a GIA model with 1D viscosity variations, for the purpose of computing mass balance estimates for Antarctica as a whole and regionally. To investigate this requires knowledge of which 1D viscosity profile corresponds best to a certain 3D viscosity distribution. However, sensitivity of the gravity rate to 3D variations in viscosity depends on the size of the load and on the viscosity itself, which are not well known. Therefore, it is difficult to average the 3D viscosity structure in a way that represents the true sensitivity of the loading process. To add to that, viscosity in our model is also a function of time. Therefore, we opt to compute gravity rates for a range of 1D models that adopt different upper and lower mantle viscosity values. We then compute the misfit between these 1D models and a 3D model, and use the model with smallest misfit as the best 1D approximation to the 3D model. For this test the ICE-5G ice model is selected as the loading history. We expect similar conclusions for other ice models, but that remains to be investigated. The gravity rates of 1D models are computed using the spectral model of van der Wal et al. (2011). Differences in spatial resolution between the FE model and the spectral model lead to small differences in predictions, as demonstrated in supplementary material A.4. Misfit is computed between the 1D and 3D models for all 2° x 2° grid cells within the land area of Antarctica, accounting for the reduction in area towards the pole. The 3D models and the 1D models that best approximate them are shown in Figure 6 and mass balance estimates for the best-fitting 1D models are added to Table 2 as rows 5 to 7. The estimates for the 1D models differ from the 3D model by at most 6 Gt/year, which is within the range of previously-computed differences between a finite-element model and a spectral 1D model.

The question remains as to whether there are regional differences between a 3D model and the 1D model that best approximates it. In a 1D model the gravity rate pattern tends to resemble the distribution of total ice thickness change, even though small differences in the timing of melt might exist from one location to another. For a 3D model the pattern of total ice thickness change and the pattern of present-day gravity rates can be very different from each other.

Studying the spatial pattern in Figure 6, it can be seen that the gravity rate pattern of 3D models HF10D and S4D are quite well approximated by a 1D model; the maximum gravity rate in both the 1D and 3D models is found at Siple Dome where most of the ice thickness change since LGM took place according to ICE-5G. However, model S10W predicts the maximum gravity rate to be in the Weddell Sea, while its corresponding 1D model predicts the maximum gravity rate to be at Siple Dome. Indeed, we verified that for the ICE-5G ice model (Peltier 2004) the location of the predicted maximum uplift rate for 1D models that sample a large range of upper/lower mantle viscosity combinations always corresponds to the Siple Dome. This also holds true for the IJ05 model (compare figure 4 of Ivins and James (2005) to their figure 2) and the IJ05_R2 model (compare figures 4 and 5 of Ivins et al. 2013 with their figure 3d). Note also that the HF10D model changes the location of the maximum uplift rate for the Whitehouse et al. (2012b) model from the Weddell Sea to near the Ross Sea (Figure 5).

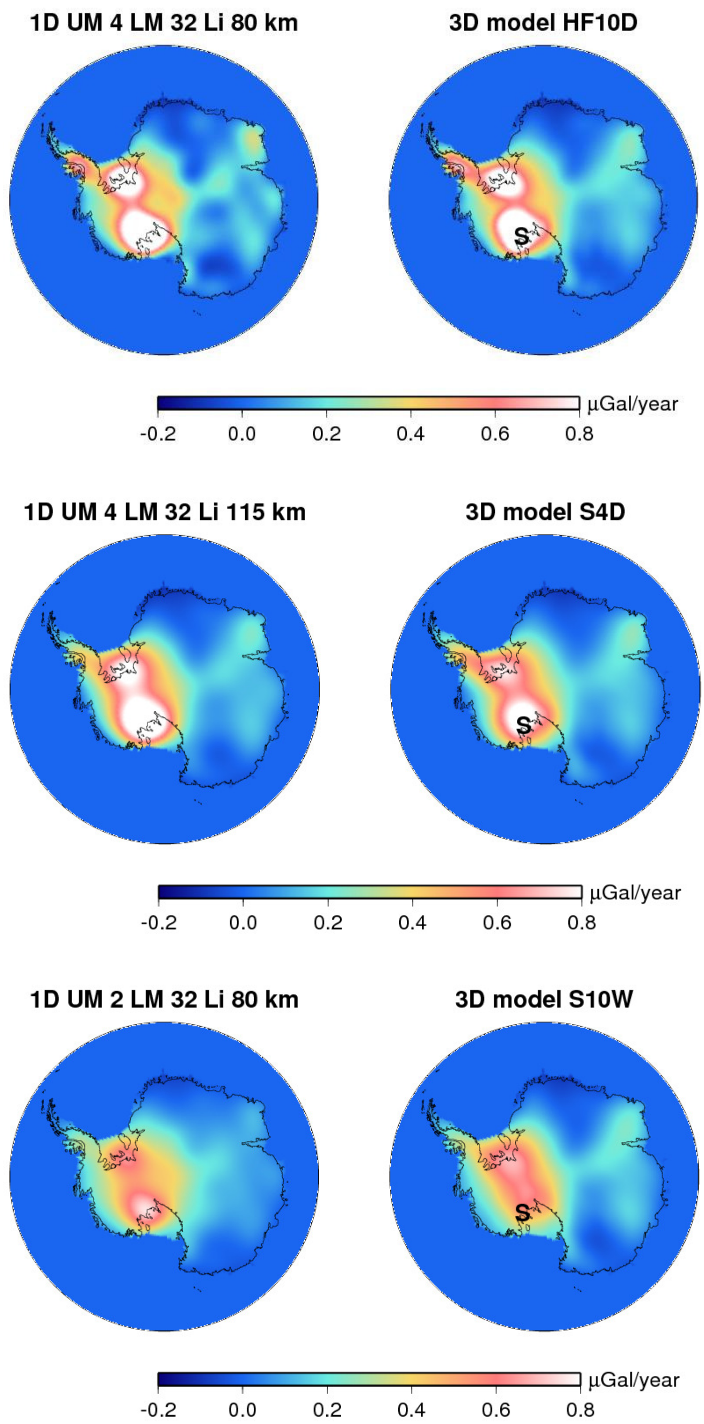

Figure 6: Free-air gravity anomaly rates for the 3D models from section 3.1 (right column) and the 1D models that best approximate them (left column). Maximum spherical harmonic degree used in both models is 90. Upper and lower mantle viscosities (UM/LM) are as indicated in the figure titles (times 10^{20} Pa s), as well as lithosphere thickness (Li). 'S' denotes the location of Siple Dome.

Conclusions

From a set of GIA models with 3D viscosity, three preferred models were selected which provided the best fit to either GPS-observed uplift rates in the northern hemisphere, or relative sea-level data in Fennoscandia. All three models include viscosity profiles that vary by several orders of magnitude within the upper mantle. The model that predicts the best-fitting uplift rates in the northern hemisphere is based on flow laws for dry olivine with large grain size (10 mm). This results in viscosity values below 10^{19} Pa s for parts of West Antarctica at 95 km depth, increasing to almost 10^{22} Pa s at 300 km depth. Viscosities that are even lower are obtained for an alternative model with a wet olivine rheology. Although using mineral flow laws to compute viscosities is uncertain, the rheological parameters for low viscosities are in agreement with xenolith findings in Antarctica which reveal grain sizes smaller than 1 mm and which show the presence of hydrous minerals in mantle rocks.

Using the 3D viscosity models to correct GRACE data (February 2003 – June 2013) for GIA effects results in Antarctic mass balance estimates of -146 to -166 Gt/year for the ICE-5G ice model and -39 to -55 Gt/year for the W12a model. These values are less negative than earlier estimates based on 1D models for the same ice loading histories. It is possible to find a 1D model that approximates the gravity rates from each of the 3D models for the purpose of GRACE mass balance estimates. However, estimates based on 3D models are outside the confidence intervals for earlier published mass balance estimates based on 1D GIA models. The variation around the mean resulting from the introduction of a range of 3D viscosity models is 10 and 8 Gt/year for ICE-5G and W12a, respectively. The reduced mean ice melt estimates as well as the variation around the mean indicates that 3D viscosity can significantly affect mass balance estimates. In practice, uncertainties associated with 3D viscosity are likely to be even greater if the trade-off between ice loading and 3D Earth rheology were taken into account during development of the ice-loading history.

For one 3D model with wet rheology (and lower effective viscosity) the predicted spatial pattern of gravity rates was markedly different to the patterns produced by the closest 1D model approximation. For example, the location of the largest gravity rate for this 3D model (based on ICE-5G) no longer corresponds to the location of greatest ice thickness change since the LGM, as is the case for 1D models. This demonstrates that future mass balance studies that use GRACE to determine the spatial distribution of ice mass change will benefit from the use of more realistic viscosity distributions within Antarctic GIA models. It also indicates that ice loading histories that have been tuned to fit GIA observations using 1D viscosity profiles may be in error.

Acknowledgements

We thank the two reviewers for their comments which helped us to improve the manuscript. We gratefully acknowledge Merijn Logtestijn for compiling the xenolith studies in S.3 and Matt King for valuable discussions regarding the GPS data. WW is funded by the Netherlands Organisation for Scientific Research. PLW is supported by a NERC Independent Research Fellowship.

References

A, G., J. Wahr and S. Zhong (2013). Computations of the viscoelastic response of a 3-D compressible Earth to surface loading: an application to Glacial Isostatic Adjustment in Antarctica and Canada. Geophys. J. Int. 192(2): 557-572.

Andronikov, A.V. (1990). Spinel-garnet lherzolite nodules from alkaline-ultrabasic rocks of Jetty Peninsula (East Antarctica). Antarctic Science 2(4):321-330.

Argus, D.F., W.R. Peltier, R. Drummond and A.W. Moore (2014). The Antarctica component of postglacial rebound model ICE-6G_C (VM5a) based on GPS positioning, exposure age dating of ice thicknesses, and relative sea level histories. Geophys. J. Int. 198(1): 537-563.

Barletta, V.R., R. Sabadini and A. Bordoni (2008). Isolating the PGR signal in the GRACE data: impact on mass balance estimates in Antarctica and Greenland. Geophys. J. Int. 172(1): 18-30.

Barnhoorn, A., W. van der Wal and M.R. Drury (2011a). Upper mantle viscosity and lithospheric thickness under Iceland. J. Geodyn. 52(3-4): 260-270.

Barnhoorn, A., W. van der Wal, L.L.A. Vermeersen and M.R. Drury, (2011b). Lateral, radial, and temporal variations in upper mantle viscosity and rheology under Scandinavia, Geochem. Geophy. Geosy., 12, Q01007.

Boening, C., M. Lebsock, F. Landerer and G. Stephens (2012). Snowfall-driven mass change on the East Antarctic ice sheet. Geophys. Res. Lett. 39(21): L21501.

Cammarano, F., P. Tackley, and L. Boschi (2011). Seismic, petrological and geodynamical constraints on thermal and compositional structure of the upper mantle: global thermochemical models, Geophys. J. Int., 187(3): 1301-1318.

Chen, J. L., C.R. Wilson, D. Blankenship and B.D. Tapley (2009). Accelerated Antarctic ice loss from satellite gravity measurements. Nat. Geosci. 2(12): 859-862.

Cheng, M., B.D. Tapley and J.C. Ries, (2013). Deceleration in the Earth's oblateness, J. Geophys. Res. - Sol. Ea., 118: 740-747, doi: 10.1002/jgrb.50058.

Coltorti, M., L. Beccaluva, C. Bonadiman, B. Faccini, T. Ntaflos and F. Siena (2004). Amphibole genesis via metasomatic reaction with clinopyroxene in mantle xenoliths from Victoria Land, Antarctica. Lithos 75: 115–139.

Danesi, S. and A. Morelli (2001). Structure of the upper mantle under the Antarctic Plate from surface wave tomography. Geophys. Res. Lett. 28(23): 4395-4398.

Dijkstra, A.H., M.R. Drury and R.M. Frijhoff (2002). Microstructures and lattice fabrics in the Hilti mantle section (Oman Ophiolite): Evidence for shear localization and melt weakening in the crust–mantle transition zone? J. Geophys. Res. 107 (2270), doi:10.1029/2001JB000458.

Dziewonski, A.M. and D.L. Anderson (1981). Preliminary reference Earth model. Physics of The Earth and Planetary Interiors 25(4): 297-356.

Farrell, W.E. and J.A. Clark (1976). On postglacial sea level. Geophys. J. Roy. Astr. S., 46: 647-667.

Faul, U. H., and I. Jackson (2005), The seismological signature of temperature and grain size variations in the upper mantle, Earth Planet. Sc. Lett., 234(1–2): 119-134.

Foley, S.F., A.V. Andronikov, D.E. Jacob and S. Melzer (2006). Evidence from Antarctic mantle peridotite xenoliths for changes in mineralogy, geochemistry and geothermal gradients beneath a developing rift. Geochim. et Cosmochim. A. 70: 3096–3120.

Gasperini, P., D.A. Yuen and R. Sabadini (1992). Postglacial rebound with a non-newtonian upper mantle and a newtonian lower mantle rheology. Geophys. Res. Lett. 19(16): 1711-1714.

Gemelli, M., S. Rocchi, G. Di Vincenzo and M. Petrelli, M. (2009). Accretion of juvenile crust at the Early Palaeozoic Antarctic margin of Gondwana: geochemical and geochronological evidence from granulite xenoliths. Terra Nova 21: 151–161.

Grand, S.P. (2002). Mantle shear-wave tomography and the fate of subducted slabs, Philos. Trans. R. Soc. Lond., A, 360: 2475–2491.

Gunter, B. C., O. Didova, R.E.M. Riva, S.R.M. Ligtenberg, J.T.M. Lenaerts, M.A. King, M.R. van den Broeke and T. Urban (2014). Empirical estimation of present-day Antarctic glacial isostatic adjustment and ice mass change. The Cryosphere 8(2): 743-760.

Handler, M.R., R.J. Wysoczanski and J.A. Gamble (2003). Proterozoic lithosphere in Marie Byrd Land, West Antarctica: Re–Os systematics of spinel peridotite xenoliths. Chemical Geology 196: 131– 145.

Hirth, G. and D. Kohlstedt (2003). Rheology of the Upper mantle and the mantle wedge: a view from the experimentalists, in: Eiler, J. (Ed.), Inside the Subduction Factory, Geophysical Monograph Series 138. American Geophysical Union, Washington, DC, 83-105.

Ivins, E.R. and T.S. James (2005). Antarctic glacial isostatic adjustment: a new assessment. Antarct. Sci. 17(4): 537-549.

Ivins, E.R. and C.G. Sammis (1995). On lateral viscosity contrast in the mantle and the rheology of low-frequency geodynamics. Geophys. J. Int. 123(2): 305-322.

Ivins, E.R., M.M. Watkins, D.-N. Yuan, R. Dietrich, G. Casassa and A. Rülke (2011). On-land ice loss and glacial isostatic adjustment at the Drake Passage: 2003–2009. J. Geophys. Res. - Sol. Ea. 116(B2): B02403.

Ivins, E. R., T.S. James, J. Wahr, E.J.O. Schrama, F.W. Landerer and K.M. Simon (2013). Antarctic contribution to sea level rise observed by GRACE with improved GIA correction. J. Geophys. Res. - Sol. Ea. 118(6): 3126-3141.

Karato, S.-i. (2008). Deformation of Earth Materials, Cambridge University Press, Cambridge, UK, 463 pp.

Kaufmann, G., P. Wu and E.R. Ivins (2005). Lateral viscosity variations beneath Antarctica and their implications on regional rebound motions and seismotectonics. J. Geodyn. 39(2): 165-181.

Keary, P., K.A., Klepeis and F.J. Vine (2009). Global Tectonics, 3rd Edition, Wiley-Blackwell, West Sussex, UK, 463 pp.

King, M.A., R.J. Bingham, P. Moore, P.L. Whitehouse, M.J. Bentley and G.A. Milne (2012). Lower satellite-gravimetry estimates of Antarctic sea-level contribution. Nature 491(7425): 586-589.

Lidberg, M., J.M. Johansson, H.-G. Scherneck and J.L. Davis, (2007). An improved and extended GPS-derived 3D velocity field of the glacial isostatic adjustment (GIA) in Fennoscandia, J. Geodesy 81: 213–230.

Markl, G., R. Abart, T. Vennemann, and H. Sommer (2003). Mid-crustal Metasomatic Reaction Veins in a Spinel Peridotite. J. Petrol. 44(6): 1097-1120.

Milne, G.A. and J.X. Mitrovica (1998). Postglacial sea-level change on a rotating Earth, Geophys. J. Int. 133: 1-19.

Nield, G. A., P.L. Whitehouse, M.A. King, P.J. Clarke and M.J. Bentley (2012). Increased ice loading in the Antarctic Peninsula since the 1850s and its effect on glacial isostatic adjustment. Geophys. Res. Lett. 39(17): L17504.

Nield, G.A., V.R. Barletta, A. Bordoni, M.A. King, P.L. Whitehouse, P.J. Clarke, E. Domack, T.A. Scambos and E. Berthier (2014). Rapid bedrock uplift in the Antarctic Peninsula explained by viscoelastic response to recent ice unloading. Earth Planet. Sc. Lett. 397(0): 32-41.

Peltier, W.R. (2004). Global Glacial Isostasy and the Surface of the Ice-Age Earth: The ICE-5G (VM2) Model and Grace. Annu. Rev. Earth Planet. Sci. 32: 111-149.

Peltier, W.R., R. Drummond and K. Roy (2012). Comment on Ocean mass from GRACE and glacial isostatic adjustment by D.P. Chambers et al. J. Geophys. Res. - Sol. Ea. 117(B11): B11403.

Perinelli, C., P. Armienti and L. Dallai, (2011). Thermal Evolution of the Lithosphere in a Rift Environment as Inferred from the Geochemistry of Mantle Cumulates, Northern Victoria Land, Antarctica. J. Petrol., 52(4) 665-690.

Perinelli, C., G.B. Andreozzi, A.M. Conte, R. Oberti and P. Armienti (2012). Redox state of subcontinental lithospheric mantle and relationships with metasomatism: insights from spinel peridotites from northern Victoria Land (Antarctica). Contrib. Mineral. Petr. 164: 1053–1067.

Pollack, H.N., S.J. Hurter and J.R. Johnson (1993). Heat flow from the Earth's interior: Analysis of the global data set, Rev. Geophys. 31: 267-280.

Rodell, M., P. R. Houser, U. Jambor, J. Gottschalck, K. Mitchell, C.-J. Meng, K. Arsenault, B. Cosgrove, J. Radakovich, M. Bosilovich, J.K. Entin, J.P. Walker, D. Lohmann and D. Toll (2004). The global land data assimilation system, Bull. Am. Meteorol. Soc. 85, 3, 381-394.

Ritzwoller, M.H., N.M. Shapiro, A.L. Levshin and G.M. Leahy (2001). Crustal and upper mantle structure beneath Antarctica and surrounding oceans. J. Geophys. Res. - Sol. Ea. 106(B12): 30645-30670.

Riva, R.E.M., B.C. Gunter, T.J. Urban, L.L.A. Vermeersen, R.C. Lindenbergh, M.M. Helsen, J.L. Bamber, R.S.W. van de Wal, M.R. van den Broeke and B.E. Schutz (2009). Glacial Isostatic Adjustment over Antarctica from combined ICESat and GRACE satellite data. Earth Planet. Sc. Lett. 288(3-4): 516-523.

Sasgen, I., H. Konrad, E.R. Ivins, M.R. Van den Broeke, J.L. Bamber, Z. Martinec and V. Klemann (2013). Antarctic ice-mass balance 2003 to 2012: regional reanalysis of GRACE satellite gravimetry measurements with improved estimate of glacial-isostatic adjustment based on GPS uplift rates. The Cryosphere 7(5): 1499-1512.

Schaeffer A.J. and Lebedev, S (in press).. Global heterogeneity of the lithosphere and underlying mantle: A seismological appraisal based on multimode surface-wave dispersion analysis, shear-velocity tomography, and tectonic regionalization. The Earth's Heterogeneous Mantle, Springer.

Schrama, E.J.O., B. Wouters and R. Rietbroek (2014). A mascon approach to assess ice sheet and glacier mass balances and their uncertainties from GRACE data, J. Geophys. Res. - Sol. Ea. 119(7): 6048-6066, doi:10.1002/2013JB010923

Sella, G.F., S. Stein, T.H. Dixon, M. Craymer, T.S. James, S. Mazzotti, S. and R.K. Dokka, (2007). Observation of glacial isostatic adjustment in “stable” North America with GPS, Geophys. Res. Lett. 34, L02306, doi:10.1029/2006GL027081.

Shapiro, N.M. and M.H. Ritzwoller (2004). Inferring surface heat flux distributions guided by a global seismic model: particular application to Antarctica. Earth Planet. Sc. Lett. 223(1-2): 213-224.

Shepherd, A., et al. (2012). A Reconciled Estimate of Ice-Sheet Mass Balance. Science 338(6111): 1183-1189.

Shuman, C.A., H.J. Zwally, B.E. Schutz, A.C. Brenner, J.P. DiMarzio, V.P. Suchdeo and H.A. Fricker (2006). ICESat Antarctic elevation data: Preliminary precision and accuracy assessment. Geophys. Res. Lett. 33(7): L07501.

Thomas, I. D., M. A. King, M.J. Bentley, P.L. Whitehouse, N.T. Penna, S.D.P. Williams, R.E.M. Riva, D.A. Lavallee, P.J. Clarke, E.C. King, R.C.A. Hindmarsh and H. Koivula (2011). Widespread low rates of Antarctic glacial isostatic adjustment revealed by GPS observations. Geophys. Res. Lett. 38(22): L22302.

Trampert, J. and R.D. van der Hilst (2005). Towards a quantitative interpretation of global seismic tomography. In: van der Hilst, R.D., et al. (Eds.), Earth’s Deep Mantle: Structure, Composition and Evolution, Geophysical Monograph, vol. 160. American Geophysical Union, pp. 47–62.

van der Wal, W., P. Wu, H. Wang and M. G. Sideris (2010). Sea levels and uplift rate from composite rheology in glacial isostatic adjustment modeling. J. Geodyn. 50(1): 38-48.

van der Wal, W., E. Kurtenbach, J. Kusche and L.L.A. Vermeersen (2011). Radial and tangential gravity rates from GRACE in areas of glacial isostatic adjustment, Geophys. J. Int. 187: 797–812.

van der Wal, W., A. Barnhoorn, P. Stocchi, S. Gradmann, P. Wu, M. Drury and B. Vermeersen (2013). Glacial isostatic adjustment model with composite 3-D Earth rheology for Fennoscandia. Geophys. J. Int. 194 (1): 61-77.

Velicogna, I. and J. Wahr (2006). Measurements of Time-Variable Gravity Show Mass Loss in Antarctica. Science 311(5768): 1754-1756.

Velicogna, I. (2009). Increasing rates of ice mass loss from the Greenland and Antarctic ice sheets revealed by GRACE. Geophys. Res. Lett. 36(19): L19503.

Wahr, J., H. DaZhong, and A. Trupin (1995), Predictions of vertical uplift caused by changing polar ice volumes on a viscoelastic Earth, *Geophys. Res. Lett.*, 22(8), 977-980, doi:10.1029/94GL02840.

Wahr, J., D. Wingham and C. Bentley (2000). A method of combining ICESat and GRACE satellite data to constrain Antarctic mass balance. J. Geophys. Res. - Sol. Ea. 105(B7): 16279-16294.

Wang, H., L. Jia, H. Steffen, P. Wu, L. Jiang, H. Hsu, L. Xiang, Z. Wang, and B. Hu (2013), Increased water storage in North America and Scandinavia from GRACE gravity data, Nature Geosci, 6(1), 38-42.

Warner, R.D. and P.J. Wasilewski (1995). Magnetic petrology of lower crust and upper mantle xenoliths from McMurdo Sound, Antarctica. Tectonophysics 249: 69-92.

Whitehouse, P.L., M.J. Bentley and A.M. Le Brocq (2012a). A deglacial model for Antarctica: geological constraints and glaciological modelling as a basis for a new model of Antarctic glacial isostatic adjustment. Quaternary Sci. Rev. 32(0): 1-24.

Whitehouse, P.L., M.J. Bentley, G.A. Milne, M.A. King and I.D. Thomas (2012b). A new glacial isostatic adjustment model for Antarctica: calibrated and tested using observations of relative sea-level change and present-day uplift rates, Geophys. J. Int., 190(3): 1464-1482.

Wu, P. (2004). Using commercial finite element packages for the study of earth deformations, sea levels and the state of stress. Geophys. J. Int. 158(2): 401-408.

Wu, P., H. Wang, and H. Steffen (2013). The role of thermal effect on mantle seismic anomalies under Laurentia and Fennoscandia from observations of Glacial Isostatic Adjustment, Geophys. J. Int., 192(1): 7-17.

Wu, X., M.B. Heflin, H. Schotman, L.L.A. Vermeersen, D. Dong, R.S. Gross, E.R. Ivins, A.W. Moore and S.E. Owen (2010). Simultaneous estimation of global present-day water transport and glacial isostatic adjustment. Nat. Geosci. 3(9): 642-646.

Wysoczanski, R.J., J.A. Gamble, P.R. Kyle and M.F. Thirlwall (1995). The petrology of lower crustal xenoliths from the Executive Committee Range, Marie Byrd Land Volcanic Province, West Antarctica. Lithos 36: 185-201.

Zipfel, G. and G. Wörner (1991). Four- and five-phase peridotites from a continental rift system: evidence for upper mantle uplift and cooling at the Ross Sea margin (Antarctica). Contrib. Mineral. Petr. 111: 24-36.

Highlights

- GIA model with 3D viscosity based on seismic tomography and olivine flow laws.
- Low viscosities ($< 10^{19}$ Pa s) beneath West Antarctica.
- Significantly affected spatial pattern of uplift rate.
- Smaller mass loss for Antarctica found from GRACE data.